Karki, Sabin Kumar; Ala-Laurinaho, Juha; Viikari, Ville

Comparison of Additively Manufactured Dual-Polarized Probe Antennas at Ku-Band

Published in:
2023 International Workshop on Antenna Technology, iWAT 2023

DOI:
10.1109/iWAT57058.2023.10171622

Published: 01/01/2023

Document Version
Peer-reviewed accepted author manuscript, also known as Final accepted manuscript or Post-print

Please cite the original version:
Karki, S. K., Ala-Laurinaho, J., & Viikari, V. (2023). Comparison of Additively Manufactured Dual-Polarized Probe Antennas at Ku-Band. In *2023 International Workshop on Antenna Technology, iWAT 2023* IEEE. https://doi.org/10.1109/iWAT57058.2023.10171622

Comparison of Additively Manufactured Dual-Polarized Probe Antennas at Ku-Band

Sabin Kumar Karki*†, Juha Ala-Laurinaho*, and Ville Viikari*
Department of Electronics and Nanoengineering, Aalto University, FI-00076 AALTO, Finland, juha.ala-laurinaho@aalto.fi
†Currently: Huawei Technologies Finland, 00180 Helsinki, Finland

***Abstract*—This paper presents a comparison between two additively manufactured dual-polarized open-ended waveguide probe antennas. The probe antenna design covers the up-link and down-link frequencies of satellite communications at Ku-band (10.7 – 14.5 GHz), and it could be used for fast ground-station antenna measurements. The used fabrication processes are the fused filament fabrication (FFF) followed by the metallization with conductive paint and the direct metal printing using binder-jet process. The measured performance of the manufactured prototypes agrees well with the simulated performance in the design frequency range. The slight dimensional deviations from the design values increase the low-frequency coupling and reflection coefficients compared to the simulations. To decrease the coupling between polarizations, a horn-type waveguide opening is introduced.**

***Index Terms*—additive manufacturing, probe antenna, orthomode transducer, square waveguide**

I. Introduction

Additive manufacturing (AM) or 3D-printing is the process of fabricating a structure with the theme of combining materials together. In the past decades, the rapid development in additive manufacturing (AM) technology has made antenna prototyping easier and more common [1]. Furthermore, AM allows to realize complex structural details which are difficult make with conventional manufacturing methods. There are several AM processes such as stereolithography (SLA), selective laser melting (SLM), fused filament fabrication (FFF) or fused deposition modeling (FDM), electron beam melting, and binder-jet pirnting [1]. Using these AM processes, the desired structures can be realized with plastic, ceramic, and metals. However, most of the commonly available 3D printers support only dielectric materials. Typically, metal-AM services are provided by limited professional institutions and fabrication time is longer. Nevertheless, numerous antennas are manufactured using metal AM [2], [3]. Metal structures may offer mechanical strength and can bear high temperatures. High weight of the metal-AM produced components is a disadvantage in many commercial applications.

Recently, various processes for the metallization of plastic-AM parts are studied [4]–[6]. The most commonly used processes are taping, electroplating, electroless plating, conductive paint coating, and ink-jet printing [4], [5], [7]–[9]. Using, e.g., adhesive copper tape to metallize the plastic parts is easy and fast, however, as the structures become complicated the taping may be impossible [7] and the limited adhesive conductivity may break galvanic contact in tape overlapping areas. The electroplating process deposits a layer of metal on the plastic parts which is pre-treated with galvanic coating [5]. According to [4], the electroplating process can achieve good conductivity, but the metal deposition might be non-uniform [5]. Electroless plating can achieve a uniform and thick metal layer in complex geometries and cavities at a low-cost, but the process may be slow [8]. The inkjet printer can deposit a metal layer on a dielectric substrate [9], [10]. However, to achieve good conductivity, the printed parts need to be sintered at high temperature, approx. 125°-150°C, which needs to be considered when choosing materials.

An easy and efficient alternative for the metallization is spraying or painting with conductive paint [5]–[7]. Specialized machines are often used to ensure controlled thickness [11]. In [4], the gain and efficiency of the prototype with conductive paint are comparable with the electroplated prototype in an 8-18 GHz frequency range. The impedance matching and gain of the slot antenna paintbrush-coated with liquid conductive silver paint is comparable with the commercial silver-metallization service [6].

Recently, a comparison between a plastic-SLA-printed and copper-electroplated horn and an aluminum-SLM-printed horn at mm-waves was presented [12]. In this work, however, different plastic-AM and metal-AM processes for antenna manufacturing are compared: binder-jet metal (BJM) printing with stainless steel and FFF-based plastic printing followed by coating with conductive paint. Stainless steel BJM is reported to provide better dimensional accuracy than aluminum-SLM-printing [2]. On the other hand, FFF followed by metal painting is a low-cost fabrication method. The studied antenna is a dual-polarized probe antenna designed for Ku-band. The corresponding dimensions and RF properties, i.e. impedance matching, gain, and radiation pattern, are compared. Further, a horn-type waveguide opening is proposed to decrease coupling between two polarizations.

II. Dual-polarized probe

The design and operation of the coaxial-fed dual-polarized probe antenna (DPP) based on the square waveguide are detailed in [13]. The DPP consists of a grating polarizer-based orthomode transducer (OMT) and an open-ended waveguide (OEWG) as the radiating element as shown in Fig. 1. The side length of the designed square OEWG is 14.55 mm for

This work was partly funded by Business Finland through RF Sampo project (3071/31/2021).

2023 International Workshop on Antenna Technology (iWAT) | 979-8-3503-3408-1/23/$31.00 ©2023 IEEE | DOI: 10.1109/iWAT57058.2023.10171622

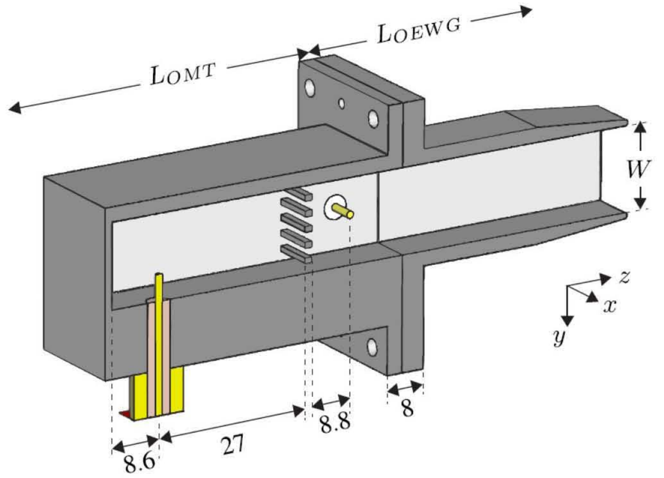

Fig. 1: (a) Cut-away view of the proposed dual-polarized probe. Dimensions are in mm.

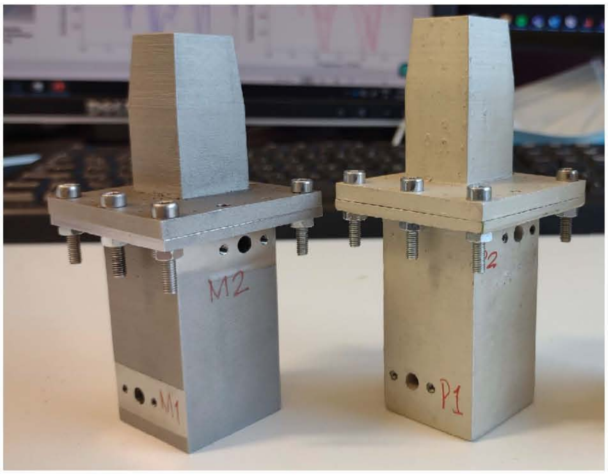

Fig. 2: Dual-polarized probe antennas fabricated with binder-jet metal-printing process (left) and FFF plastic printing followed by coating with conductive paint (right).

TABLE I: Comparison of the DPP dimension. Dimensions are in mm.

Dimensions	Plastic printing + Conductive paint	Binder-jet metal printing	Designed value
L_{OMT}	55	54	55
L_{OEWG}	42.25	41.5	42.25
W	14.6	14.25-14.45	14.55

the operation in the Ku-band, i.e. 10.7-14.5 GHz covering the up-link and down-link frequencies of satellite communications [14]. The DPP could be used for fast ground-station antenna measurements. The OEWG end is trimmed to minimize the scattering [15]. The DPP structure includes a rather detailed OMT structure requiring high manufacturing accuracy and is therefore considered feasible for the comparison between two AM processes.

III. Fabrication

The dual-polarized probe is manufactured in two parts, OMT and OEWG, instead of a single part as in [13]. The main reason is due to the limited volumetric capacity of the binder-jet printing service, but it also eases the application of the conductive paint. A flange with alignment and screw holes is used to align and assemble the OMT and OEWG. The used manufacturing processes are described in the following sections.

A. Binder-jet metal printing

The prototype manufactured with binder-jet metal printing using Stainless steel 316 L is shown in Fig. 2. The manufacturer ensures that the average surface roughness is 6 µm and the expected conductivity of the material is 1.8×10^6 S/m [16]. The dimensions of the manufactured prototype are within the $\pm 2\%$ tolerance limit provided by the manufacturer. However, almost all the dimensions of the OMT and OEWG are smaller than the designed ones. The lengths of the fabricated OMT and OEWG are 54 and 41.5 mm, respectively, which are 1 and 0.75 mm smaller than the design values, see Table I. The cross-sectional dimension of the square waveguide also varies between 14.28 and 14.45 mm, meaning that the cross-section of the waveguide is slighty trapezoidal. Furthermore, the flange surfaces of both the OMT and OEWG are milled to flatten the surfaces for improved connection and alignment which further reduced the overall length of the DPP. The weight of the metal-AM prototype parts is 350 g without flange screws and connectors.

B. Plastic printing and coating with conductive paint

The prototype is also manufactured in-house with plastic printing or FFF process using Polylactic acid (PLA) filaments. The surface roughness of plastic parts manufactured with FFF process is approx. 15 µm and the manufacturing resolution is approx. 10 µm [17]. The measured dimensions are well in line with the design values, see Table I.

The metallization of the plastic-AM prototype is done with MG Chemicals 842WB conductive paint whose conductivity is $\sigma = 1.3 \times 10^6$ S/m [11]. The surface of the plastic printed parts is made slightly coarse with sandpaper before the conductive paint is applied with a paintbrush. Three layers of conductive paint are applied on the plastic parts at an interval of eight hours to achieve consistent metal thickness greater than skin depth which is 5 µm at 10.5 GHz. The weight of the plastic-AM parts is 58 g without flange screws and connectors. Based on visual observation, the surface roughness of the FFF plastic parts decreases after applying conductive paint. In [18], the average surface roughness is reported to be 8.5 µm after manually applying the silver paint on the plastic parts printed with SLA process.

IV. Simulation and Measurement Results

A. Comparison between the DPP prototypes

Two panel-mount SMA connectors are attached to each of the DPP prototypes for the measurements. For both prototypes,

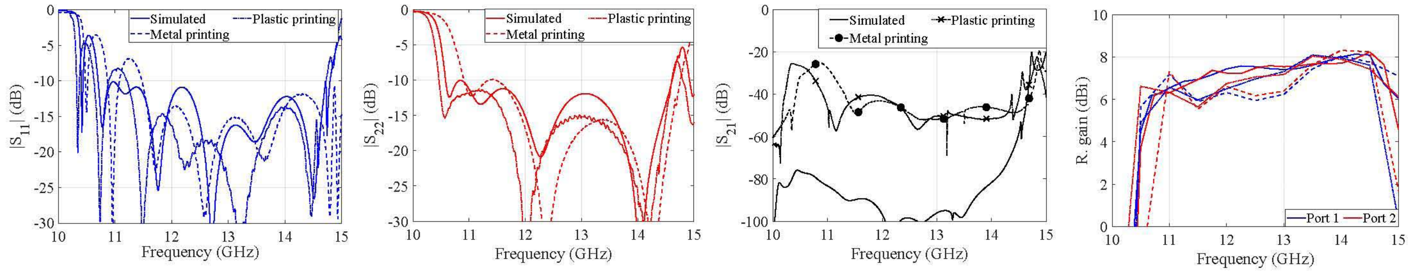

(a) (b) (c) (d)

Fig. 3: Simulated and measured reflection coefficients of (a) Port 1 and (b) Port 2, and (c) coupling between the ports, and (d) realized gains (line-types as in (a) and (b)) of the plastic-AM and metal-AM DPPs.

the walls of the OMTs are increased to achieve the correct coaxial probe length of 4.5 mm inside the waveguide. Fig. 3 shows the measured and simulated scattering parameters: reflection coefficients and coupling between the ports. The level of the reflection coefficients are similar, but at the low-frequency end of the band there are discrepancies both between the prototypes and in comparison with the simulated result. The metal-printed prototype has the highest cut-off frequency which is accounted for the smallest OEWG aperture size.

The measured coupling between the ports is clearly larger than the simulated coupling for the both prototypes. The simulated value is mostly below −80 dB. To achieve this in practice would require extremely accurate fabrication. Thus, the measured level of −40 dB over most of the band is considered good. The coupling of the both prototypes is higher at about 10.5–11 GHz. The potential reason for the high coupling is assumed to be the impedance mismatch at the radiating aperture of OEWG. The peak coupling levels of the two prototypes offset in frequency which might be due to the difference in the OEWG aperture dimensions. A solution to the impedance mismatch at radiating aperture is discussed in the next sub-section. Fig. 3 (d) shows the measured and simulated realized gains. The overall gain levels are similar although the conductivity of the Stainless steel used in the simulation is 7×10^6 S/m is greater than the conductivities of the prototype metals, as discussed in sections III A and B. At the center of the band, the fabricated prototypes exhibit somewhat lower gains, the largest discrepancy being about 1.5 dB whereas at the low- and high-end of the band the realized gain is similar.

Fig. 4 shows the normalized measured radiation patterns with a comparison to the simulation results. For both ports, at the frequency range of 10.7-14 GHz (not all frequency points shown), the measured co-polarized patterns are symmetric and agree well with simulations. At frequency close to 14.5 GHz, both the simulated and measured radiation patterns are asymmetric, see Fig. 4 (b) and (d), due to the effect of the higher order mode [13]. In the case of plastic-AM DPP, which has larger cross-section of the OEWG and lower cut-off frequency of TE_{11}, the measured radiation pattern is more asymmetric than in the simulation, see Fig. 4 (b). In contrast, the measured radiation pattern of the metal-AM DPP is more symmetric because the OEWG cross-section is smaller, see Fig. 4 (d). The maximum cross-polarization radiation of the plastic-AM and metal-AM DPP is 25 dB and 18 dB, respectively. The cross-polar radiation for both the prototypes reaches maximum at 11 GHz, which suggest that high cross-polar coupling between port 1 and 2 at lower frequencies may also increase the cross-polar radiation.

B. Horn-type waveguide opening

In order to reduce coupling, the square OEWG is substituted with the horn-shaped radiating element as shown in Fig. 5. The radiating element is manufactured with the same plastic-AM process as explained in Section III B. The measured S-parameters of the DPP with OEWG and horn as the radiating element is shown in Fig. 6. The plastic-AM OMT is used in both measurements. The horn-shaped radiating element improves the impedance matching at frequencies closer to cut-off, i.e., around 11 GHz. Fig. 6 (b) shows that the coupling between the orthogonal polarizations improves significantly around 11 GHz with the horn-shaped radiating element as compared to OEWG.

CONCLUSION

The additive manufacturing of a dual-polarized antenna with an OMT was studied. A plastic-printed antenna coated with conductive paint and directly metal-printed antenna were prototyped. The OMTs and radiating parts realized with the same AM methods were connected through flanged waveguide connections. The performance of the manufactured probe antennas were in line with the simulated performance. The largest deviation was observed in the coupling between the differently-polarized ports, which is considered as the most sensitive parameter for the manufacturing errors. However, the coupling was mostly below −40 dB. The coupling could be further improved through horn-like radiating part by reducing the reflection from the aperture-air interface. The performance of the both realized prototypes is considered well feasible for the Ku-band.

ACKNOWLEDGMENT

The authors would like to thank Mr. Matti Vaaja for machining the flange surfaces of the metal-printed prototype.

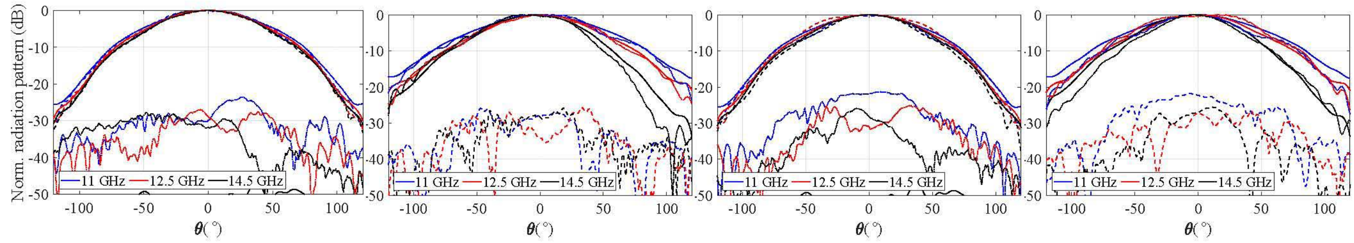

(a) (b) (c) (d)

Fig. 4: Simulated (y-pol:—, x-pol: - · · -) and measured (y-pol: - - -, x-pol: · · ·) normalized radiation patterns in the xz-plane for (a) Port 1 (H-plane) and (b) Port 2 (E-plane) of the plastic-AM DPP, and (c) Port 1 (H-plane) and (d) Port 2 (E-plane) of the metal-AM DPP.

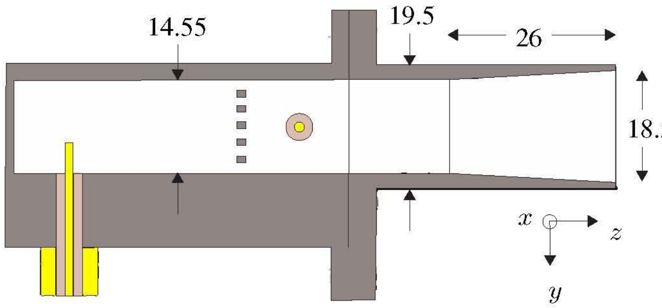

Fig. 5: (a) Cut-away view of the proposed DPP with horn radiating element. Dimensions are in mm.

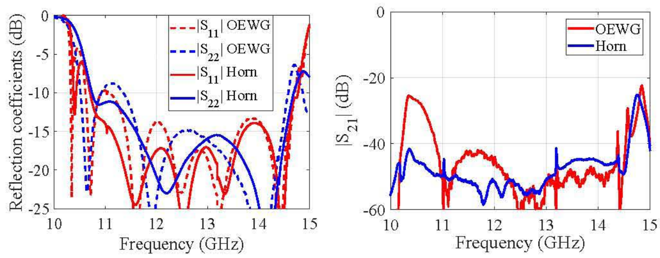

(a) (b)

Fig. 6: Measured (a) reflection coefficients and (b) couplings for plastic-AM DPPs with OEWG- and horn-type radiating elements.

References

[1] D. Helena, A. Ramos, T. Varum, and J. N. Matos, "Antenna design using modern additive manufacturing technology: A review," *IEEE Access*, vol. 8, pp. 177 064–177 083, 2020.

[2] H. Kähkönen, S. Proper, J. Ala-Laurinaho, and V. Viikari, "Comparison of additively manufactured and machined antenna array performance at Ka-band," *IEEE Antennas and Wireless Propagation Letters*, vol. 21, no. 1, pp. 9–13, 2022.

[3] B. Zhang and *et al.*, "Metallic 3-D printed antennas for millimeter- and submillimeter wave applications," *IEEE Transactions on Terahertz Science and Technology*, vol. 6, no. 4, pp. 592–600, 2016.

[4] K. V. Hoel, S. Kristoffersen, J. Moen, K. G. Kjelgård, and T. S. Lande, "Broadband antenna design using different 3D printing technologies and metallization processes," in *2016 10th European Conference on Antennas and Propagation (EuCAP)*, 2016, pp. 1–5.

[5] K. Lomakin and *et al.*, "Evaluation and characterization of 3-D printed pyramid horn antennas utilizing different deposition techniques for conductive material," *IEEE Transactions on Components, Packaging and Manufacturing Technology*, vol. 8, no. 11, pp. 1998–2006, 2018.

[6] S. Alkaraki, Y. Gao, S. Stremsdoerfer, E. d. Gayets, and C. Parini, "3D printed antennas metallized using conductive paint at X-band," in *2019 13th European Conference on Antennas and Propagation (EuCAP)*, 2019, pp. 1–5.

[7] H. Yao, S. Sharma, R. Henderson, S. Ashrafi, and D. MacFarlane, "Ka band 3D printed horn antennas," in *2017 Texas Symposium on Wireless and Microwave Circuits and Systems (WMCS)*, 2017, pp. 1–4.

[8] E. G. Geterud, P. Bergmark, and J. Yang, "Lightweight waveguide and antenna components using plating on plastics," in *2013 7th European Conference on Antennas and Propagation (EuCAP)*, 2013, pp. 1812–1815.

[9] B. K. Tehrani, R. A. Bahr, W. Su, B. S. Cook, and M. M. Tentzeris, "E-band characterization of 3D-printed dielectrics for fully-printed millimeter-wave wireless system packaging," in *2017 IEEE MTT-S International Microwave Symposium (IMS)*, 2017, pp. 1756–1759.

[10] M. F. Farooqui and A. Shamim, "3-D inkjet-printed helical antenna with integrated lens," *IEEE Antennas and Wireless Propagation Letters*, vol. 16, pp. 800–803, 2017.

[11] M. Chemicals, "842WB Liquid," MG Chemicals datasheet, Surrey, BC, Canada, Tech. Rep., Dec. 2022. [Online]. Available: https://www.mgchemicals.com/downloads/tds/tds-842wb-l.pdf

[12] A. Vaske, A. Akar, and B. Neubauer, "Coplanar waveguide fed U-band horn antenna manufactured using 3D printing and electroplating," in *2022 16th European Conference on Antennas and Propagation (EuCAP)*, 2022, pp. 1–4.

[13] S. K. Karki, J. Ala-Laurinaho, and V. Viikari, "Dual-polarized probe for planar near-field measurement," *IEEE Antennas and Wireless Propagation Letters*, pp. 1–5, 2022.

[14] ETSI, "Satellite Earth Stations and Systems (SES); Harmonised Standard for fixed and in-motion Earth Stations communicating with non-geostationary satellite systems (NEST) in the 11 GHz to 14 GHz frequency bands covering essential requirements of article 3.2 of Directive 2014/53/EU," European Telecommunications Standards Institute, Tech. Rep., Dec. 2017. [Online]. Available: https://www.etsi.org/deliver/etsi_en/303900_303999/303980/01.01.01_60/en_303980v010101p.pdf

[15] E. H. Ko and D. J. Belgiovane, "Radiation and scattering pattern characteristics of chamfered-tip open-ended rectangular waveguide probes for planar near-field antenna measurement applications," in *2021 Antenna Measurement Techniques Association Symposium (AMTA)*, 2021, pp. 1–5.

[16] Digital Metal. [Online]. Available: https://digitalmetal.tech

[17] D.-K. Ahn, S.-M. Kwon, and S.-H. Lee, "Expression for surface roughness distribution of FDM processed parts," in *2008 International Conference on Smart Manufacturing Application*, 2008, pp. 490–493.

[18] T. Freialdenhoven, P. Witte, S. Koß, J. H. Schleifenbaum, and T. Dallmann, "Different metallization techniques using a 3D printed E-band orthomode transducer," in *2021 51st European Microwave Conference (EuMC)*, 2022, pp. 342–345.